Aalborg Universitet

Model Predictive Control of PMSG-Based Wind Turbines for Frequency Regulation in an Isolated Grid

Wang, Haixin; Yang, Junyou; Chen, Zhe; Ge, Weichun; Ma, Yiming; Xing, Zuoxia; Yang, Lijian

Published in:
IEEE Transactions on Industry Applications

DOI (link to publication from Publisher):
10.1109/TIA.2018.2817619

Publication date:
2018

Document Version
Accepted author manuscript, peer reviewed version

Link to publication from Aalborg University

Citation for published version (APA):
Wang, H., Yang, J., Chen, Z., Ge, W., Ma, Y., Xing, Z., & Yang, L. (2018). Model Predictive Control of PMSG-Based Wind Turbines for Frequency Regulation in an Isolated Grid. *IEEE Transactions on Industry Applications*, *54*(4), 3077-3089. https://doi.org/10.1109/TIA.2018.2817619

General rights
Copyright and moral rights for the publications made accessible in the public portal are retained by the authors and/or other copyright owners and it is a condition of accessing publications that users recognise and abide by the legal requirements associated with these rights.

- Users may download and print one copy of any publication from the public portal for the purpose of private study or research.
- You may not further distribute the material or use it for any profit-making activity or commercial gain
- You may freely distribute the URL identifying the publication in the public portal -

Take down policy
If you believe that this document breaches copyright please contact us at vbn@aub.aau.dk providing details, and we will remove access to the work immediately and investigate your claim.

Downloaded from vbn.aau.dk on: May 02, 2026

This article has been accepted for publication in a future issue of this journal, but has not been fully edited. Content may change prior to final publication. Citation information: DOI 10.1109/TIA.2018.2817619, IEEE Transactions on Industry Applications

Model Predictive Control of PMSG-Based Wind Turbines for Frequency Regulation in an Isolated Grid

Haixin Wang, Junyou Yang, Zhe Chen, *Senior Member*, *IEEE*, Weichun Ge, Yiming Ma, Zuoxia Xing and Lijian Yang

***Abstract*—This paper proposes a frequency regulation strategy applied to wind turbine generators (WTGs) in an isolated grid. In order to complement active power shortage caused by load or wind speed change, an improved deloading method is proposed to improve the regulation capabilities in different speed sections and to provide WTG power reserves. Considering torque compensation may cause power fluctuation, speed reference of conventional pitch control system should be reset. Moreover, to suppress disturbances caused by load and wind speed as well as overcome dependence on system parameters, a model predictive controller (MPC) is presented to generate torque compensation for each deloaded WTG, which allows each WTG to react to the disturbance differently, depending on its generator speed and the frequency deviation. Hardware-in-the-loop simulation and experimental results show that the proposed strategy can enhance frequency response ability during load changes and smoothen power fluctuations resulting from wind speed variations.**

***Index Terms*—Deloading method, frequency regulation, model predictive control (MPC), torque compensation control, wind turbine generator (WTG).**

NOMENCLATURE

$P_{e,farm}$	Wind farm output power
i	Index for WTGs, i=1, 2, 3, 4
$P_{e,i}$	Output power of WTG i
P_m	Mechanical power of WTG
$P_{e,nom}$	The rated power of WTG
P_{dev}	Power deviation
P_d	Diesel generator output power
P_l	Load power
V_w	Wind speed
$V_{w,i}$	Wind speed of WTG i
ρ	Density of air
C_p	wind power utilization coefficient
λ	Tip speed ratio
β	Pitch angle
A_r	Swept area of wind turbine
c_1, c_2, c_3, c_4, c_5, c_6	Fitting coefficients
T_e	Electric magnetic torque
$T_{e,i}$	Electric magnetic torque of WTG i
$T_{e,nom}$	The rated torque of WTG
T_m	Mechanical torque of WTG
$T_{e,com}$	Torque compensation
$T_{e,comi}$	Torque compensation of WTG i
$T_{e,deli}$	Deloading torque of WTG i
k_{opt}	Optimal factor
ω_r	Angular speed
$\omega_{r,i}$	Angular speed of WTG i
ω_0	Cut-in angular speed
ω_1	Initial angular speed of transition section
$\omega_{r,nom}$	The rated speed of WTG
$\omega_{r,max}$	The speed up limit
ω_r^*	Speed reference of pitch system
τ_β	Mechanical time constant of pitch servo
M	Inertia coefficient of synchronous generator
D	Load damping coefficient
H	Inertia coefficient of WTG
T_d, T_g	Mechanical time constants of engine and governor respectively
K_I	Integral coefficient of diesel generator
R	Droop factor of diesel generator
k_f, k_{f1}, k_{f2}	Deloading factors
K_P	Variable droop factor
f, f_{dev}	Isolated grid frequency and frequency deviation
$f_{dev}(k+1\|k)$	Predictive value of frequency deviation at instant k
$f_{dev,m}(k+1\|k)$	Modified predictive value of frequency deviation
μ	Correction factor
ε, α	Weights of error of frequency deviation and torque compensation in the performance evaluation function respectively
$T_{e,i}^{\min}$, $T_{e,i}^{\max}$	Minimum and maximum of torque of WTG i
$T_{e,comi}^{\min}$, $T_{e,comi}^{\max}$	Minimum and maximum of torque compensation of WTG i
$f_{dev}^{\min}$, $f_{dev}^{\max}$	Minimum and maximum of frequency deviation

Manuscript received September 20, 2017. This research is supported by "Application Technology Research and Engineering Demonstration Program of National Energy" of China (NY20150303).

Haixin Wang, Junyou Yang, Yiming Ma and Zuoxia Xing are with School of Electrical Engineering, Shenyang University of Technology, Shenyang 110870, China (e-mail: sutxny_whx@126.com; junyouyang@sut.edu.cn; sutxny_mym@126.com; xingzuox@163.com).

Zhe Chen is with Department of Energy Technology, Aalborg University, Denmark, (zch@et.aau.dk).

Weichun Ge is with Liaoning Province Electric Power Company, Shenyang 110006, China (gwc@In.sgcc.com.cn).

Lijian Yang is with School of Information Science and Engineering, Shenyang University of Technology, Shenyang 110870, China (yanglijian888@163.com).

0093-9994 (c) 2018 IEEE. Personal use is permitted, but republication/redistribution requires IEEE permission. See http://www.ieee.org/publications_standards/publications/rights/index.html for more information.

This article has been accepted for publication in a future issue of this journal, but has not been fully edited. Content may change prior to final publication. Citation information: DOI 10.1109/TIA.2018.2817619, IEEE Transactions on Industry Applications

$P_{e,farm}^{\min}, P_{e,farm}^{\max}$ Minimum and maximum of output power
$\Delta P_{e,farm}$ Active power change

I. INTRODUCTION

IN an isolated grid containing wind turbine generators (WTGs) and conventional synchronous generators, frequency stability is a key index which is commonly supported by the synchronous generators. Due to the large installation of WTGs with a high penetration, limited synchronous generators could not be able to provide the required active power for frequency regulation. Stochastic natures of wind energy make power balance difficult. Meanwhile, load change may lead to frequency instability [1]-[3]. The limitation on the regulating ability of synchronous generator brings a serious challenge to frequency stability of an isolated grid. Consequently, there is an urgent need for WTGs to participate in regulating frequency [4], [5].

The frequency stability of isolated grid could not depend on WTGs completely. However, within a certain extent, WTGs have the ability to regulate frequency [6]-[8]. Some possible regulation schemes were proposed, such as a coordination of WTGs with energy storage system (ESS), pitch control and converter control [9], a coordinated control strategy with battery-based ESS of wind farm for supporting primary frequency [10], and combined frequency regulation strategies of WTGs with flywheels, fuel cells, ultracapacitors etc. [11]-[13]. The coordinated control method with ESS enhanced ability of regulating frequency [14]. However, in addition to the complexity of communication interactions, the required capacity and associated economic costs have to be taken into account when ESSs are used for wind farms [15], [16]. Model predictive control (MPC) was applied to the pitch system for frequency regulation in microgrid [17]. Due to the delay characteristic of pitch actuator, WTGs could not fully regulate the frequency when relying only on pitch control system.

The method of regulating frequency with converter control has the advantages of low cost, simple application and fast response. Two schemes of converter control were studied. One scheme is that WTG runs in the maximum power point tracking (MPPT) condition, and the power response to frequency variation for short time is achieved by inertia characteristic and kinetic energy. However, due to the rapid change of WTG speed, severe instability of system is easily caused [18]-[20]. Another scheme is that WTG does not track the maximum power point and the power reserve is achieved by under-speeding or over-speeding control methods. The WTG is deloaded to possess power reserves for frequency regulation in [21], [22]. Power reserves of deloaded WTGs result in energy losses. The power reserve in a high-speed section is larger than that in a low-speed section, but few studies consider to reduce the gap of frequency response capabilities in different WTG speed sections.

In terms of power response to frequency variation, the most popular control strategy applied to WTG is the variable droop control. In [23], based on the deloaded WTG, variable droop control was proposed to support an isolated grid under depressed frequency condition, but utilizing wind speed as an input variable may not be appropriate for actual applications. Furthermore, torque and power droop controllers based on linearized models of generator-side converter were compared in [24]. But the condition of over rated speed has not been considered in the linearized models. The dependence of variable droop controller on some system parameters leads to poor system stability.

Furthermore, H_∞ and μ-synthesis robust control techniques were used to develop the secondary frequency control loop [25]. But this paper focused on how to dispatch instructions to each WTG directly for primary frequency regulation. Reference [26] proposed a fuzzy-logic based frequency controller for wind farms to improve the primary frequency response. The inputs of the fuzzy-logic based frequency controller are wind speed and frequency. Reference [27] designed a central controller based on MPC and some Kalman filters to improve wind farm performance in frequency regulation. The task of Kalman filters is to estimate wind speed sent to MPC. Thus, the performances of the presented strategy depend on the accuracy of the predicted wind speed. The use of wind speed in these controllers is to obtain the possible output power of a WTG. However, in the actual practical scenario, wind speed is not suggested as an input signal of the controller. In the MPC controller presented in this paper, WTG speed is considered as a control variable instead of wind speed. Meanwhile, in order to utilize WTGs for regulating frequency actively, the presented MPC scheme of this paper has the ability of frequency prediction.

In this paper, the deloaded WTGs are adopted to regulate frequency without special ESS. To reduce the gap of inconsistent regulation capacities in different speed, an improved deloading method is presented. The operation of deloaded WTG participated in frequency regulation is different from conventional WTG. Thus, speed reference of pitch control system is reset to adjust power effectively. MPC controller is presented to compensate torque which not only enhances the anti-load disturbance ability and smoothens wind farm output in the whole range of wind speed, but also reduces the dependence on system parameters. The proposed controller mainly responds to WTG speed and frequency deviations caused by load and wind speed changes. When frequency deviation is stable at zero, the wind farm has no power compensation.

This paper is organized as follows. Section II describes the isolated grid configuration. Section III proposes the improved deloading method. Characteristics of deloaded WTG with torque compensation are analyzed in section IV. MPC is designed in Section V. The hardware-in-the-loop simulation and experimental results are shown in Section VI. Finally, the conclusion is drawn.

II. ISOLATED GRID

An isolated grid comprising of four permanent magnet synchronous generators (PMSG) based wind turbines and one diesel engine driven synchronous generator is shown in Fig. 1. Each WTG is of 1.5 MW and the diesel generator is of 5 MW.

0093-9994 (c) 2018 IEEE. Personal use is permitted, but republication/redistribution requires IEEE permission. See http://www.ieee.org/publications_standards/publications/rights/index.html for more information.

This article has been accepted for publication in a future issue of this journal, but has not been fully edited. Content may change prior to final publication. Citation information: DOI 10.1109/TIA.2018.2817619, IEEE Transactions on Industry Applications

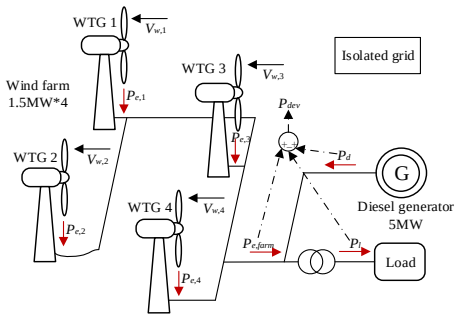

Fig. 1. Isolated grid frame.

The PMSG is connected to the isolated grid by back-to-back converter. The wind turbine model is given by (1).

$$\begin{cases} P_m = 0.5\rho C_p(\lambda,\beta)A_r V_w^3, \\ C_p(\lambda,\beta) = c_1(c_2/\lambda' - c_3\beta - c_4)e^{-c_5/\lambda'} + c_6\lambda, \\ \dfrac{1}{\lambda'} = \dfrac{1}{\lambda + 0.08\beta} - \dfrac{0.035}{\beta^3 + 1}. \end{cases} \tag{1}$$

The traditional MPPT control is to achieve the maximum wind energy of each wind turbine. The electric magnetic torque $T_{e,i}$ with MPPT control is calculated by (2) [28].

$$T_{e,i} = \begin{cases} k_{opt}\omega_{r,i}^2, & \omega_0 < \omega_{r,i} \le \omega_1 \\ \dfrac{T_{e,nom} - k_{opt}\omega_1^2}{\omega_{r,nom} - \omega_1}(\omega_{r,i} - \omega_{r,nom}) + T_{e,nom}, & \omega_1 < \omega_{r,i} < \omega_{r,nom} \\ \dfrac{P_{e,nom}}{\omega_{r,i}}. & \omega_{r,nom} \le \omega_{r,i} < \omega_{r,max} \end{cases} \tag{2}$$

In order to enhance anti-disturbance ability of the isolated grid, WTGs are deloaded to participate in regulating frequency. On the one hand, WTGs would supply power shortage when load changes suddenly. On the other hand, output power of wind farm would be smoothed. Thus, deloaded wind farm has evident advantages for improving the frequency stability.

The model of the WTG is shown in Fig. 2(a). In the pitch system, classical PI controller is to stabilize WTG speed at the reference ω_r^*. In Fig. 2(b), frequency deviation f_{dev} sent to MPC is obtained by frequency dynamic model $H_g(s)$. A central MPC controller is used to compensate torque of all WTGs and regulate frequency. Torque compensations, $T_{e,com1}$, $T_{e,com2}$, $T_{e,com3}$ and $T_{e,com4}$ are sent to each WTG. With the same control methods, the four WTGs are participated in frequency regulation. The governor and engine dynamics of the diesel generator are modeled as in [29]. To quickly compensate output power of deloaded WTG and enhance system robustness when power fluctuates in isolated grid. The electric magnetic torque is adopted as follows:

$$T_{e,i} = T_{e,deli} + T_{e,comi}. \tag{3}$$

The typical $C_p - \lambda$ curves are shown in Fig. 3. Under different pitch angles, maximum C_p curve is achieved by MPPT. Traditional WTG commonly operates at maximum C_p curve for maximum power, and deloaded WTG operates at deloading C_p curve which is on the right of maximum C_p curve. Thus,

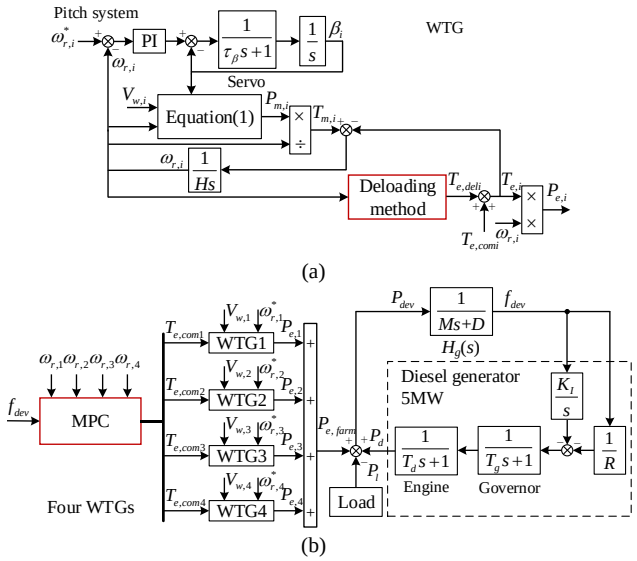

Fig. 2. (a) Model of deloaded WTG. (b) Implementation of the isolated grid for frequency regulation studies.

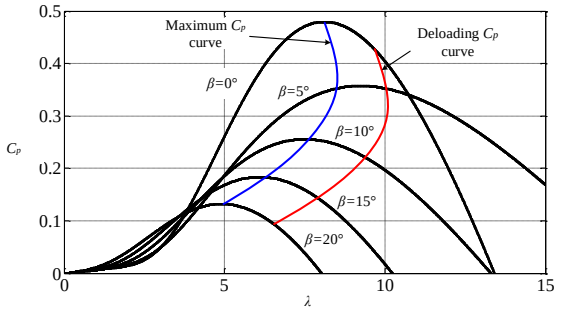

Fig. 3. The typical C_p - λ curves.

deloading C_p of WTG is increased or decreased when frequency is changed. Deloaded WTG has a certain regulating capacity based on over-speeding control [21], [22].

The power-frequency regulation of generator can be set by adjusting its control system [30], [31]. Thus, to enhance frequency stability of an isolated grid, conventional droop control method is adopted generally [32]-[34]. Reference [24] proposed torque droop controller for deloaded WTGs as follows:

$$T_e = k_f k_{opt}\omega_r^2 + K_P(f^* - f). \tag{4}$$

WTG meets power demand of isolated grid by changing the droop factor. If K_P is small, frequency modulation capability of the deloaded WTG is weakened. If K_P is great, the compensations may worsen system stable operation.

III. Deloading Method for WTGs

WTG can be deloaded to keep some power reserves for regulating frequency. Deloading factors k_{f1} and k_{f2} ($0 < k_{f1} < k_{f2} < 1$) are introduced in this paper. Corresponding relationship of torque and speed for deloaded WTG is shown in Fig. 4. The torque curve with deloading factor k_{f2} is between the torque curves with deloading factor k_{f1} and MPPT. The power regulating capacity provided with k_{f1} is larger than that with k_{f2}, while operation with MPPT would have no power reserves. The selection of deloading factors have an influence on the output power of WTG. At a wind speed higher than the rated wind

0093-9994 (c) 2018 IEEE. Personal use is permitted, but republication/redistribution requires IEEE permission. See http://www.ieee.org/publications_standards/publications/rights/index.html for more information.

This article has been accepted for publication in a future issue of this journal, but has not been fully edited. Content may change prior to final publication. Citation information: DOI 10.1109/TIA.2018.2817619, IEEE Transactions on Industry Applications

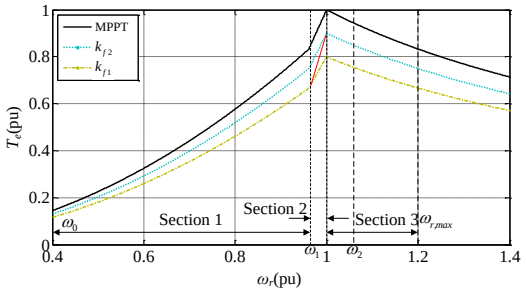

Fig. 4. The torque of WTG with different deloading factors.

speed, in order to obtain 0.1 pu power reserve, k_{f2} is selected as 0.9. k_{f1} presents higher power reserves but causes more energy loss. At a wind speed lower than the rated wind speed, k_{f2} may not be able to provide sufficient power reserve to contribute to frequency regulation. Therefore, k_{f1} may be selected as 0.8 to give more power reserves. The deloading factors may vary theoretically from 1 (no reserve) to 0 (total curtailment). The selection of deloading factors is related to capacity of a WTG and grid requirement [35]. Three specific speed sections are defined as follows.

***Section* 1**: $\omega_0 < \omega_{r,i} \le \omega_1$. Due to the less output power, the deloading factor k_{f1} in this section is selected for possessing more power reserves.

***Section* 2**: $\omega_1 < \omega_{r,i} < \omega_{r,nom}$. This section is the transition between Sections 1 and 3. The torque reference is proportional to the speed, and the red transition curve as shown in Fig. 4 is adopted for smooth output power.

***Section* 3**: $\omega_{r,nom} \le \omega_{r,i} < \omega_{r,max}$. WTG speed is higher than the rated speed, and the WTG is in the constant power state. The regulating capacity of WTG is at the highest. Thus the deloading factor k_{f2} may be selected for a certain power reserves. The power reserve of WTG in this section is larger than that in section 1.

Based on the above characteristics, the proposed deloading torque $T_{e,deli}$ is calculated by (5).

$$T_{e,deli} = \begin{cases} k_{f1} k_{opt} \omega_{r,i}^2, & \omega_0 < \omega_{r,i} \le \omega_1 \\ \dfrac{k_{f2} T_{e,nom} - k_{f1} k_{opt} \omega_1^2}{\omega_{r,nom} - \omega_1} (\omega_{r,i} - \omega_{r,nom}) + k_{f2} T_{e,nom}, & \omega_1 < \omega_{r,i} < \omega_{r,nom} \\ k_{f2} \dfrac{P_{e,nom}}{\omega_{r,i}}. & \omega_{r,nom} \le \omega_{r,i} < \omega_{r,max} \end{cases} \quad (5)$$

To analyze the performances of the deloading method, simulation of deloaded WTG is complemented with deloading factors k_{f1} and k_{f2}. The relationship between deloaded power and angular speed is shown in Fig. 5. The shaded part in Fig. 5 is the area of adjustable power from the deloaded WTG.

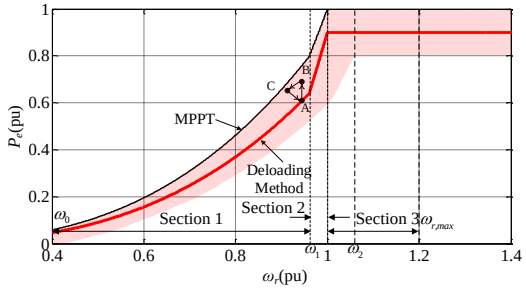

Fig. 5. The output power of deloaded WTG.

IV. Analysis of Deloaded WTG With Torque Compensation

Steady-state performances of the deloaded WTG with the compensation are simulated at different wind speeds. The simulation results are shown in Table I and Table II.

In Table I, the WTG is only deloaded without torque compensation when $T_{e,com}$ is zero. The torque and power of the deloaded WTG increase with the increase of $T_{e,com}$. At the wind speed of 10 m/s, the WTG's speed gradually decreases. At the wind speed of 13.5 m/s, the WTG operates at 1.05 pu of the rated speed by pitch control system. It can be seen from the comparison of $T_{e,com}$ with P_e, the greater absolute value of $T_{e,com}$ is, the more active power can be compensated. In the steady-state condition, the power reserve in speed section 1 is less than that in speed section 3, and inertial response would be used to obtain more available power in speed section 1 for short time. The gap of inconsistent regulation capacities between different sections is reduced, which explains the rationality of adopting different deloading factors according to speed sections.

The control laws of steady-state condition in the whole range of wind speed are shown in Fig. 6. Compared with MPPT control strategy, deloaded WTG would reach the rated speed and begin operation of pitch system when wind speed approaches the rated value. C_p with the deloading method is less than the value with MPPT. In other words, the output power of WTG is derated by keeping certain power reserve.

At under-rated wind speed, the deloaded WTG operates at point A as shown in Fig. 5. If the load increases and grid frequency decreases, WTG adjusts output power. Due to rapid increase of output power, the WTG's operation point moves to point B. Furthermore, power increase results in speed decrease, and then the operation point moves to point C. If the grid frequency deviation is stable at zero, the output power will be reduced back to point A. However, at over-rated wind speed, if the deloaded WTG increases torque to supply power shortage, and adjustment of pitch angle is not timely, the speed would be decreased from the rated value, which leads to $T_{e,del}$ decreasing and power concussion phenomenon. At this point, WTG speed

TABLE I
Output Characteristics of the Deloaded WTG at 10 m/s

$T_{e,com}$ (pu)	ω_r (pu)	T_e (pu)	P_e (pu)	Power reserve (pu)
-0.2	0.9737	0.5443	**0.5299**	**0 ~ 0.0488**
-0.1	0.9591	0.5623	**0.5393**	**-0.0094 ~ 0.0394**
0	0.9195	0.6088	**0.5598**	**-0.0299 ~ 0.0189**
0.1	0.8772	0.654	**0.5737**	**-0.0438 ~ 0.005**
0.2	0.8306	0.6967	**0.5787**	**-0.0488 ~ 0**

TABLE II
Output Characteristics of the Deloaded WTG at 13.5 m/s

$T_{e,com}$ (pu)	ω_r (pu)	T_e (pu)	P_e (pu)	Power reserve (pu)
-0.2	1.05	0.6571	**0.7**	**0 ~ 0.3**
-0.1	1.05	0.7571	**0.795**	**-0.095 ~ 0.205**
0	1.05	0.8571	**0.9**	**-0.2 ~ 0.1**
0.1	1.05	0.9571	**1**	**-0.3 ~ 0**

0093-9994 (c) 2018 IEEE. Personal use is permitted, but republication/redistribution requires IEEE permission. See http://www.ieee.org/publications_standards/publications/rights/index.html for more information.

This article has been accepted for publication in a future issue of this journal, but has not been fully edited. Content may change prior to final publication. Citation information: DOI 10.1109/TIA.2018.2817619, IEEE Transactions on Industry Applications

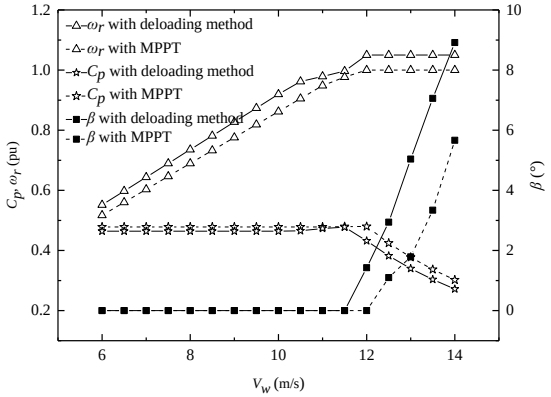

Fig. 6. The control laws of the deloaded WTG.

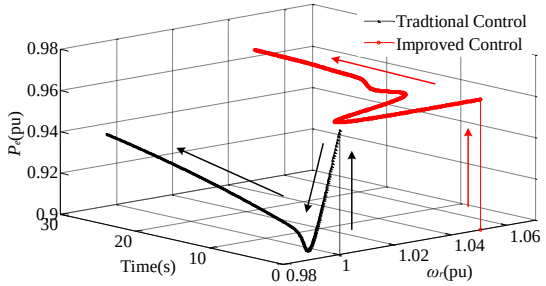

Fig. 7. Different responses of WTG when increasing torque compensation.

would be influenced by strong coupling of deloading torque controller, torque compensation controller and pitch controller. Therefore, traditional speed reference $\omega_{r,nom}$ of pitch control system is not suitable for regulating frequency, and new speed reference ω_2 of pitch control system should be set. The purpose is to ensure effectively regulating power and extend regulation time for pitch control system response.

Moreover, simulation above the rated wind speed is conducted, and results are shown in Fig. 7. The new speed reference is reset at 1.05 pu. Torque compensation is increased by 0.06 pu. With the improved control strategy, deloaded WTG increases power to 0.96 pu rapidly, and its speed has some jitter. With traditional control strategy, deloaded WTG increases power to 0.96 pu rapidly. But due to the torque compensation, WTG power is reduced immediately. It is necessary to reselect the speed reference of pitch system. The speed reference is determined by WTG performances and the maximum of torque compensation.

V. Design of Model Predictive Controller

A. Overall Description

Model predictive control adopts non-parametric model based on impulse response as the internal model. System status in the future is predicted by considering status and controls in the past and present. Then current optimal control states are obtained according to the system expected values.

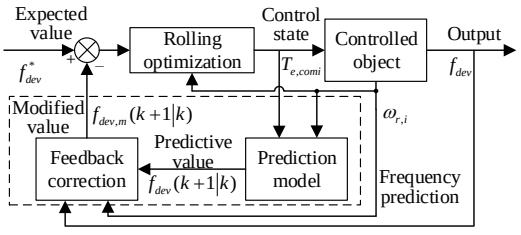

Fig. 8. Block diagram of MPC method.

MPC is essentially a kind of closed loop optimal control algorithm based on the model in the finite time horizon, which is composed of three parts: prediction model, feedback correction and rolling optimization [36]-[38]. In the sampling period T_s, the controller takes current status as initial status. Prediction results are obtained based on the prediction model, and the current optimal control states are obtained by solving a finite time optimal control problem with online rolling. In this paper, the MPC is used to predict isolated grid frequency, obtain torque compensation and inhibit frequency fluctuations. The specific block diagram of MPC is shown in Fig. 8.

B. Prediction Model and Feedback Correction

The frequency deviation in an isolated grid is calculated by (6).

$$f_{dev} = (\sum_{i=1}^{n} P_{e,i} + P_d - P_l)(\frac{1}{Ms + D}), \tag{6}$$

where $P_{e,i} = T_{e,i}\omega_{r,i}$ is output power of WTG i. Then (6) can be written as:

$$\frac{df_{dev}}{dt} = -\frac{Df_{dev}}{M} + \frac{1}{M}(\sum_{i=1}^{n} P_{e,i} + P_d - P_l). \tag{7}$$

Furthermore, according to (7), the first-order Euler discretization is obtained by (8).

$$f_{dev}(k+1|k) = (1-\frac{DT_s}{M}) f_{dev}(k) + \frac{T_s}{M}\Big[\sum_{i=1}^{n} T_{e,i}(k-1)\omega_{r,i}(k-1) + \sum_{i=1}^{n} T_{e,comi}(k)\omega_{r,i}(k) + P_d(k) - P_l(k)\Big], \tag{8}$$

where $T_{e,comi}(k)$ is the torque compensation at instant k.

Due to lack of accuracy for the prediction model system caused by sensor sampling interference and other factors in the actual system, a certain deviation between predictive frequency and actual frequency is generated. In order to improve the accuracy of predictive frequency, feedback correction is introduced by (9).

$$f_{dev,\mathrm{m}}(k+1|k) = f_{dev}(k+1|k) + x(k), \tag{9}$$

where $x(k)$ is a correction term and obtained by (10).

$$x(k) = \mu\big[f_{dev}(k) - f_{dev,\mathrm{m}}(k|k-1)\big]. \tag{10}$$

Too large or small correction factor would affect the predicted frequency. The selection of correction factor is related to the frequency prediction model. In this paper, the correction factor is 0.1.

C. Rolling Optimization

At instant k, torque compensation control target is to make the prediction of the frequency deviation as close as possible to the reference in the next instant. Meanwhile, torque compensation is expected to change appropriately, too large compensations may cause deloaded WTGs oscillation or even stop. Thus, the performance evaluation function of torque compensation control is presented in (11).

$$J(k) = \varepsilon\big[f^*_{dev}(k+1) - f_{dev,\mathrm{m}}(k+1|k)\big]^2 + \alpha\sum_{i=1}^{n} T^2_{e,\mathrm{com}\,i}(k). \tag{11}$$

Then the optimal torque compensation is transformed into

0093-9994 (c) 2018 IEEE. Personal use is permitted, but republication/redistribution requires IEEE permission. See http://www.ieee.org/publications_standards/publications/rights/index.html for more information.

This article has been accepted for publication in a future issue of this journal, but has not been fully edited. Content may change prior to final publication. Citation information: DOI 10.1109/TIA.2018.2817619, IEEE Transactions on Industry Applications

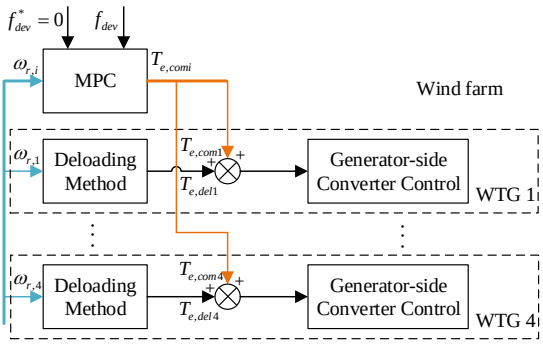

Fig. 9. Block diagram of torque compensation strategy in wind farm.

solving performance evaluation function minimization. Take the derivative of (11), and the optimal torque compensation of WTG *i* is calculated by (12).

$$T_{e,comi}(k) = \frac{\varepsilon c(k)\left[f_{dev}^*(k+1) - f_{dev}(k+1|k) - x(k)\right]}{\varepsilon c(k)^2 + \alpha}, \quad (12)$$

where $c(k) = \frac{T_s}{M}\omega_{r,i}(k)$. In addition, to make the system operation stable, the following restrictions are required in (13).

$$\begin{cases} T_{e,i}^{\min} \le T_{e,i}(k) \le T_{e,i}^{\max}, \\ T_{e,comi}^{\min} \le T_{e,comi}(k) \le T_{e,comi}^{\max}, \\ f_{dev}^{\min} \le f_{dev}(k) \le f_{dev}^{\max}. \end{cases} \quad (13)$$

At instant *k*+1, the optimization process is repeated by using the key data at *k* instant. It can be seen that the optimal torque compensation is determined by not only frequency deviation, but also WTG speed. The overall compensation control strategy of the wind farm is shown in Fig. 9.

VI. Simulation and Experiment

In order to verify the effectiveness of the proposed control strategy, simulation and experiment comparisons are conducted with MPPT control and variable droop control based on deloading method (defined as Droop) in different cases.

A. Hardware-in-the-Loop Simulation

Hardware-in-the-loop simulation platform is built as shown in Fig. 10. The wind farm, diesel generator and load are simulated by RTLAB real-time simulator, and the frequency regulation strategy is downloaded into the peripheral control panel. Technical parameters of PMSG-based wind turbines are shown in Table III.

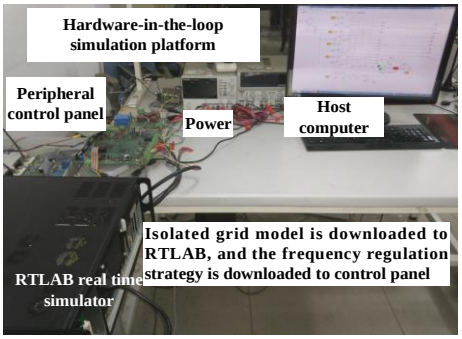

Fig. 10. Hardware-in-the-loop simulation platform.

TABLE III
Parameters of PMSG-Based on Wind Turbine

System	Parameters	Values
Wind turbine	Rated wind speed	12 m/s
	Turbine diameter	77 m
PMSG	Rated power	1.5 MW
	Rated speed	2.72 rad/s

Case 1: *all WTGs participate in frequency regulation when load changes*

The wind speeds of WTG 1, WTG 2, WTG 3 and WTG 4 are set at 10 m/s, 11 m/s, 12 m/s and 13 m/s respectively. Simulation period is 60 s. During 0-20 s, the WTGs tend to be stable gradually and load capacity is 9.25 MW. Load capacity dips to 8.25 MW at 20 s, and rises to 9.25 MW at 40 s as shown in Fig. 11(a). The simulation results are shown in Fig. 11 to Fig. 14 when wind speeds are constant.

When load changes suddenly in the isolated grid, torque compensation component of each WTG is zero with MPPT control, and output power is constant. The deloaded WTGs adjust output power with torque compensation control. In Fig. 11(b), at constant wind speed, wind farm output power is 5 MW with MPPT control. Wind farm with Droop and MPC adjusts output power at 20 s and 40 s. It can be seen that the wind farm output responds to frequency deviation. When load changes and frequency deviation increases, WTGs regulate output power until frequency deviation back to zero. The diesel generator outputs are shown in Fig. 11(c). The power change of diesel generator is the largest when WTGs with MPPT control. When WTGs adopt MPC, the power fluctuation of diesel generator is minimized. Frequency deviations with different control methods are shown in Fig. 11(d). As a result of no torque compensation, frequency deviation with MPPT control is the biggest, and the deviation amplitude with MPC is reduced to a minimum. The torque compensations of WTGs are shown in Fig. 12. The torque compensations are reduced from 20 s and

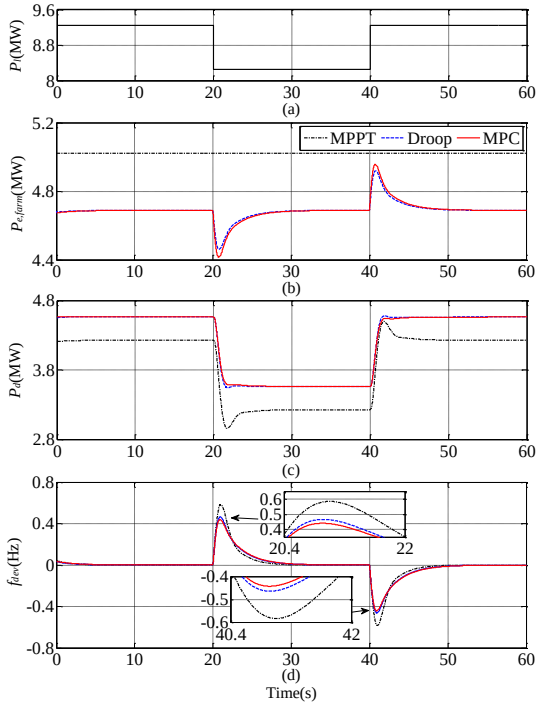

Fig. 11. Simulation results when all WTGs participate in frequency regulation.

0093-9994 (c) 2018 IEEE. Personal use is permitted, but republication/redistribution requires IEEE permission. See http://www.ieee.org/publications_standards/publications/rights/index.html for more information.

This article has been accepted for publication in a future issue of this journal, but has not been fully edited. Content may change prior to final publication. Citation information: DOI 10.1109/TIA.2018.2817619, IEEE Transactions on Industry Applications

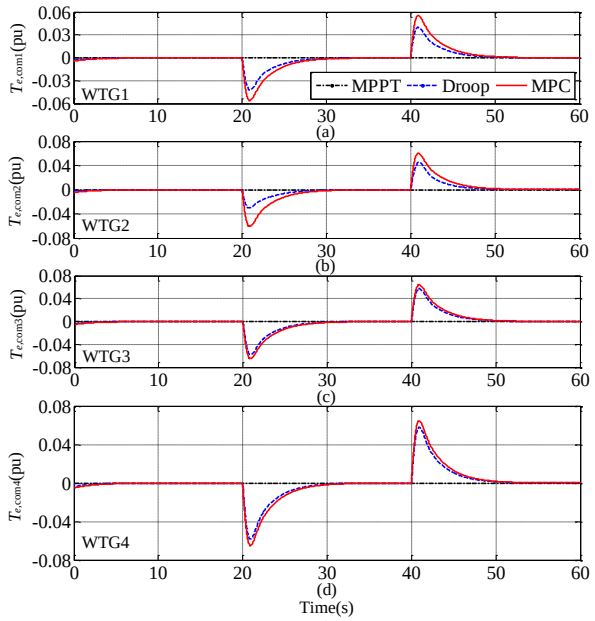

Fig. 12. Torque compensation waveforms when all WTGs participate in frequency regulation.

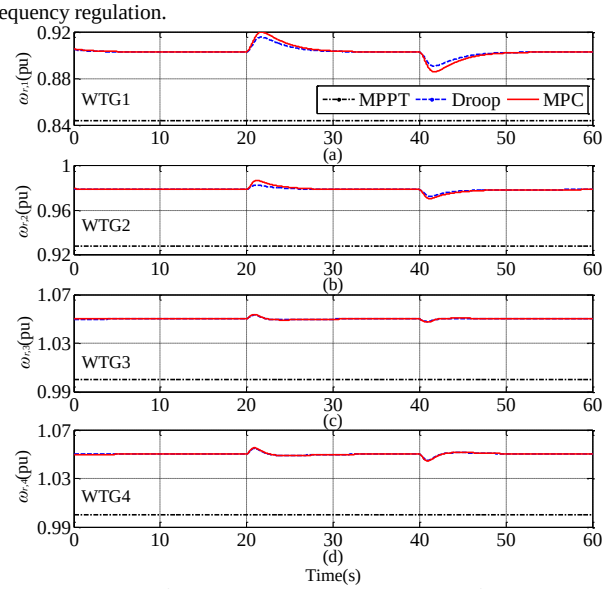

Fig. 13. Speed waveforms when all WTGs participate in frequency regulation.

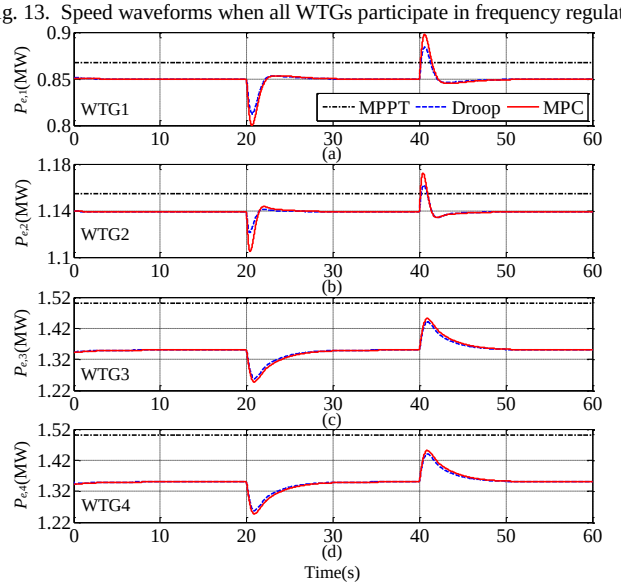

Fig. 14. Power waveforms when all WTGs participate in frequency regulation.

increased from 40 s with Droop and MPC. The maximum amplitude of compensation is about 0.06pu with MPC. The minimums of torque compensation of WTGs with MPC are -0.056 pu, -0.060 pu, -0.065 pu and -0.065 pu, the maximums of torque compensation with MPC are 0.055 pu, 0.060 pu, 0.064 pu and 0.064pu respectively. The compensations with MPC are determined by frequency deviation and the WTG speeds. However, the compensations with Droop control are not relatively strong, and they rely too much upon the droop factors. Speed waveforms of WTGs with MPPT control are constant in Fig. 13. Due to the torque compensations, WTG speeds are changed correspondingly with Droop and MPC. WTG 1 operates in section 1, WTG 2 operates in section 2, WTG 3 and WTG 4 operate in section 3. Outputs of WTGs with MPC and Droop control are reduced at 20 s, and increased at 40 s as shown in Fig. 14. The power compensations of WTGs in section 3 are larger than those in sections 1 and 2. Due to the power reserves and inertias of WTG 1 and WTG 2, their outputs with MPC and Droop control are more than those with MPPT control during a short period. The power amplitudes of four WTGs with MPC are slightly higher than those with Droop control. Compared with Droop control, the torque compensations and regulating redundancies with MPC are higher.

Case 2: *two WTGs participate in frequency regulation when load changes*

In this case, the simulation condition is set to the same as Case 1. In order to take the different number of WTGs into action for comparison, only WTG 3 and WTG 4 participate in frequency regulation. The simulation results are shown in Fig. 15 to Fig. 18.

Load change is shown in Fig. 15(a). When load changes

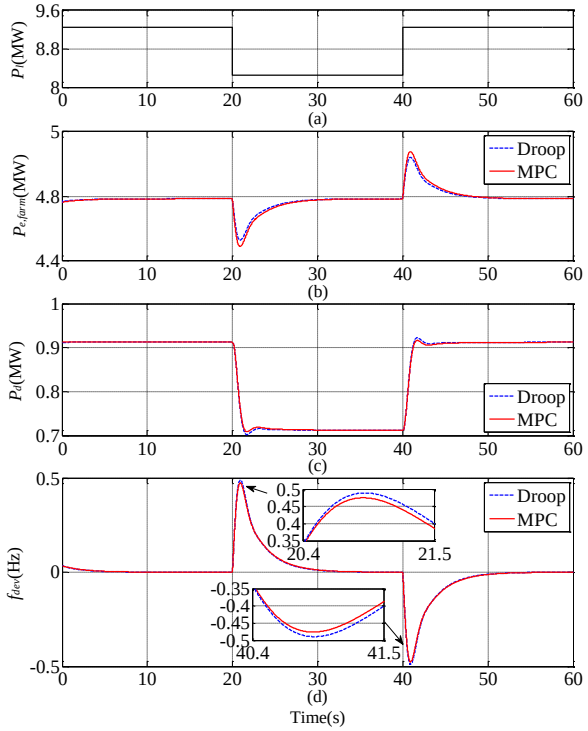

Fig. 15. Simulation results when two WTGs participate in frequency regulation.

0093-9994 (c) 2018 IEEE. Personal use is permitted, but republication/redistribution requires IEEE permission. See http://www.ieee.org/publications_standards/publications/rights/index.html for more information.

This article has been accepted for publication in a future issue of this journal, but has not been fully edited. Content may change prior to final publication. Citation information: DOI 10.1109/TIA.2018.2817619, IEEE Transactions on Industry Applications

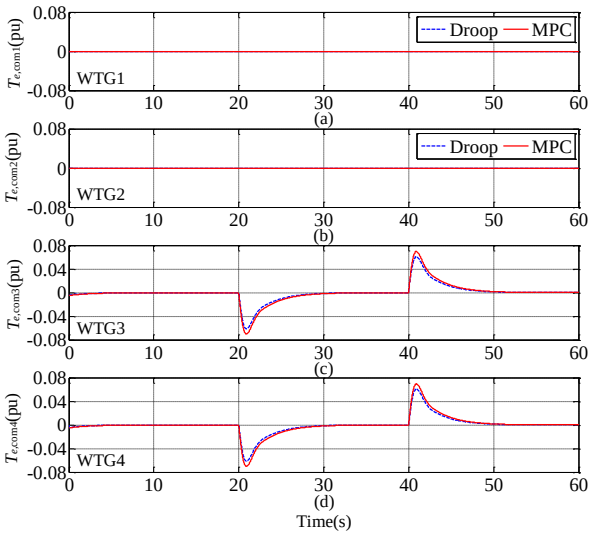

Fig. 16. Torque compensation waveforms when two WTGs participate in frequency regulation.

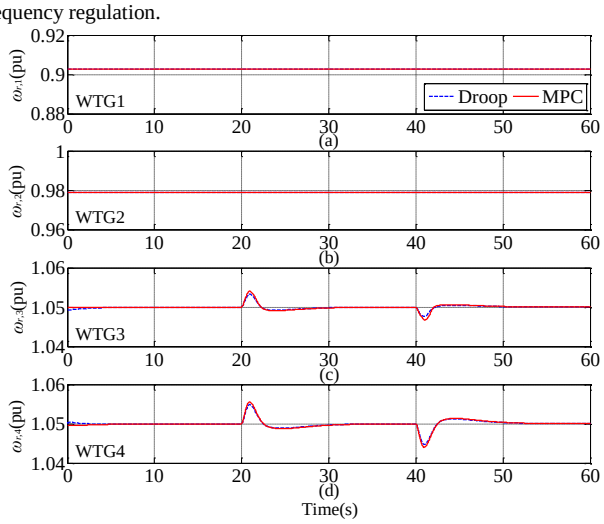

Fig. 17. Speed waveforms when two WTGs participate in frequency regulation.

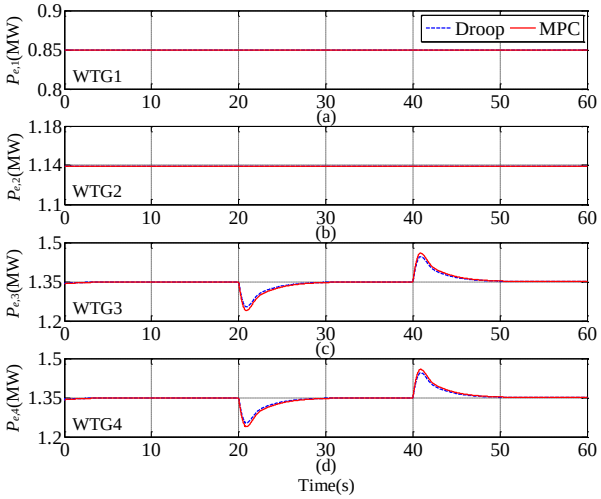

Fig. 18. Power waveforms when two WTGs participate in frequency regulation.

suddenly, two WTGs regulate output power to suppress frequency change. The difference of frequency deviation in Fig. 11(d) and Fig. 15(d) is not evident. The simulation results of four WTGs are shown in Fig. 16 to Fig. 18. It can be seen, the torque compensation components, angular speed, and output power of WTGs 1 and 2 are constant, because WTGs 1 and 2 do not participate in the frequency regulation action, the outputs of WTG 3 and 4 are slightly more than that in case 1.

Due to reduction number of WTG into action, especially the WTGs under the rated wind speed, the frequency disturbance has a little difference between Cases 1 and 2. More importantly, WTGs 1 and 2 could operate stably.

Case 3: *wind speed change*

Load power is constant as shown in Fig. 19(a), a transient wind is used in all WTGs as shown in Fig. 19(b), and the

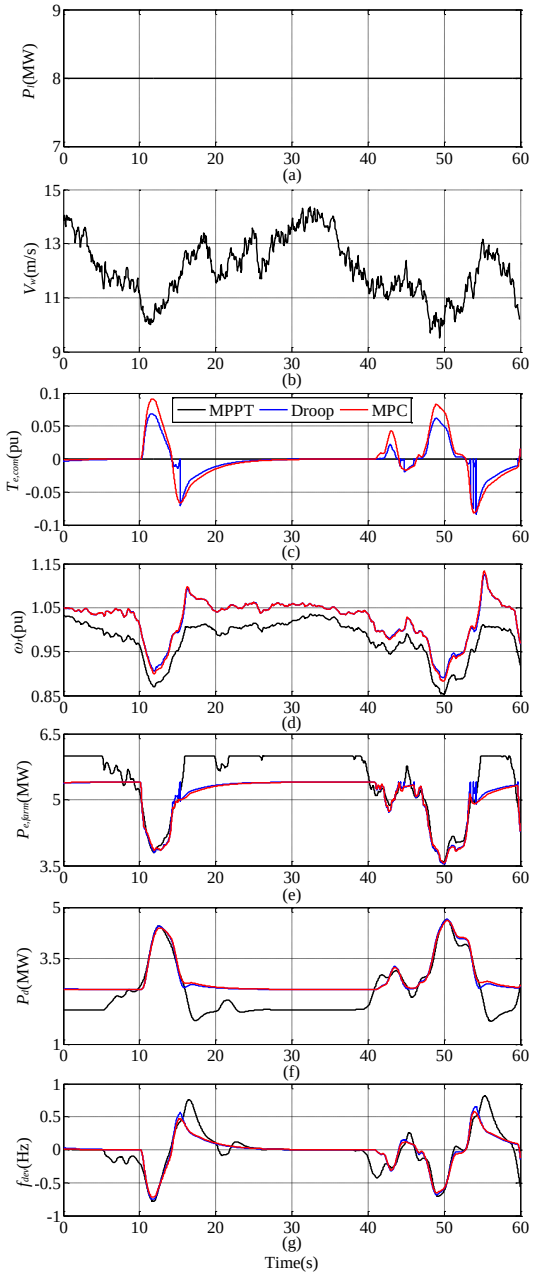

Fig. 19. Simulation results when speed changes.

TABLE IV
THE ACTIVE POWER CHANGES OF WIND FAREM

Control Strategy	$P_{e,farm}^{\min}$ (MW)	$P_{e,farm}^{\max}$ (MW)	$\Delta P_{e,farm}$ (MW)
MPPT	3.586	6	**2.414**
Droop	3.532	5.4	**1.868**
MPC	3.568	5.4	**1.832**

0093-9994 (c) 2018 IEEE. Personal use is permitted, but republication/redistribution requires IEEE permission. See http://www.ieee.org/publications_standards/publications/rights/index.html for more information.

This article has been accepted for publication in a future issue of this journal, but has not been fully edited. Content may change prior to final publication. Citation information: DOI 10.1109/TIA.2018.2817619, IEEE Transactions on Industry Applications

simulation period is 60 s. The simulation results are shown in Fig. 19. The wind speed change results in fluctuations of WTGs output power, and grid frequency is influenced. If MPPT control is applied to WTGs, frequency deviation is the largest due to less torque compensation. When frequency fluctuates, the deloaded WTGs with MPC and Droop control compensate torque to suppress frequency fluctuation.

In Fig. 19(c), the torque compensations of deloaded WTGs with MPC in three periods exhibit strong anti-disturbance ability. The torque compensation performance with Droop control is weak and depends on parameters strongly. The WTG speed curves are shown in Fig. 19(d). In order to realize regulating smoothly between sections 2 and 3, the speeds of deloaded WTGs are stabilized at 1.05 pu when wind speed is above the rated value. Deloaded wind farm increases output when wind speed decreases, and vice versa. That is, the deloaded WTGs restrain output power fluctuation caused by wind speed. As shown in Fig. 19(e), wind farm output with MPPT control is reduced at 5 s, and deloaded wind farm output is not changed. In the two periods of 10 s - 25 s and 40 s - 60 s, the power fluctuations of the wind farm with MPPT control are larger than the deloaded wind farm. It can be seen that the deloaded wind farm with MPC is better than Droop control in inhibiting power fluctuation. The output power of wind farm with MPC is smoothened. When MPC is applied to wind farm, power fluctuation of diesel generator is smaller than the other two control strategies as shown in Fig. 19(f). The frequency deviation waveforms are shown in Fig. 19(g). The frequency deviation of deloaded wind farm with MPC is the least, which shows that MPC has stronger frequency suppression ability. Meanwhile, the active power change $\Delta P_{e,farm}$ with different strategies of wind farm in 60 s are shown in Table IV. The $\Delta P_{e,farm}$ with MPC is the smallest. Compared with Droop control, the wind farm with MPC has the advantages of inhibiting wind power fluctuation and anti-disturbance ability.

In summary, the WTGs with MPPT control do not have the ability to regulate frequency. Compared with Droop control, the proposed deloaded WTGs with MPC have the advantages of inhibiting wind power fluctuation and anti-disturbance ability.

B. *Experiment*

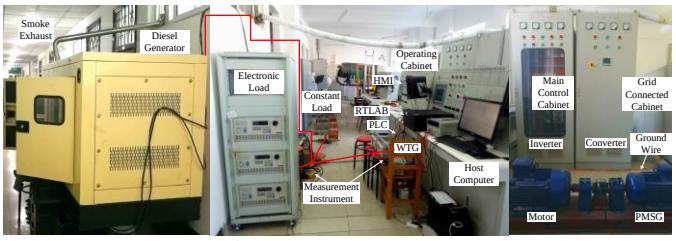

Fig. 20. Experimental platform.

TABLE V
PARAMETERS OF ISOLATED GRID

System	Parameters	Values
Diesel generator	Rated power	10 kW
	Rated frequency	50 Hz
Constant load	Rated power	5.5 kW
Electronic load	Rated power	10 kW
Wind turbine	Rated speed	12 m/s
PMSG	Rated power	10 kW

Experimental platform is shown in Fig. 20. The platform mainly includes diesel generator, constant load, electronic load, one indoor WTG and RTLAB real-time simulator. The constant load is to imitate conventional load. Load change can be achieved by the electronic load. The WTG includes operating cabinet, grid connected cabinet and main control cabinet. The wind turbine simulation is realized by the PLC. The motor drives PMSG. Isolated grid voltage data is collected into RTLAB real-time simulator for obtaining frequency. Torque compensation controller is implemented in the RTLAB. Finally, torque compensation signals are sent to the PLC through analog interfaces. Technical parameters are shown in Table V.

The frequency regulation dead zone is set at 0.18 Hz. When frequency deviation outside the dead zone, the torque compensation signals are enabled. Once frequency deviation restores to regulation dead zone, the present compensation value is held in the compensation controller.

Case 1*:* V_w=13.5 m/s

In order to compare control effects of different methods when load changes, constant wind speed is assumed, and experimental period is 10 s. At 4 s, load demand is increased by 1.5 kW. The experimental results are shown in Fig. 21.

The experimental results with MPPT control are shown in Figs. 21(a) and (b). When the load increases at 4s, frequency deviation dips (-0.64 Hz), the WTG output power is about 10 kW. The output power change of diesel generator is the most. The deloaded WTG output power is 9 kW and the power reserve is 1 kW. With Droop control, the deloaded WTG adjusts output power according to frequency deviation as shown in Figs. 21(c) and (d). The maximum output power is

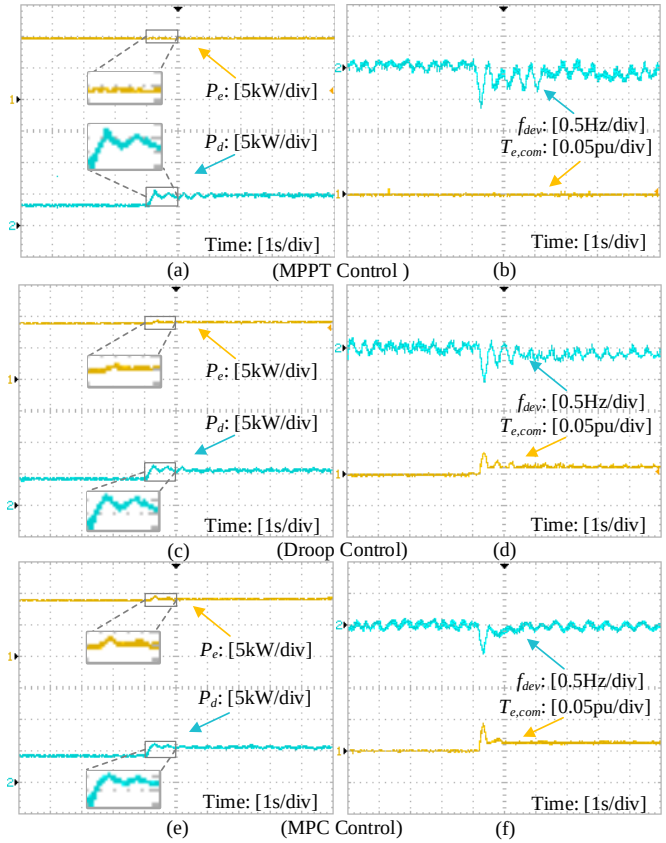

Fig. 21. Experimental results when V_w=13.5 m/s.

0093-9994 (c) 2018 IEEE. Personal use is permitted, but republication/redistribution requires IEEE permission. See http://www.ieee.org/publications_standards/publications/rights/index.html for more information.

This article has been accepted for publication in a future issue of this journal, but has not been fully edited. Content may change prior to final publication. Citation information: DOI 10.1109/TIA.2018.2817619, IEEE Transactions on Industry Applications

about 9.34 kW and the frequency deviation is reduced to -0.52 Hz. With MPC control, the maximum output power is about 9.45 kW, and the minimum frequency deviation is -0.48 Hz as shown in Fig. 21(f). When the load changes, the power compensation of WTG to the isolated grid is the largest, and the output power change of diesel generator is the smallest. The anti-disturbance ability of isolated grid is enhanced.

Case 2: wind speed change

Wind speed is shown in Fig. 22(a), load capacity is constant, and experimental period is 100 s. Experimental results are shown in Fig. 22. To restrain frequency fluctuation caused by wind speed change, WTG increases output power when wind speed decreases, and vice versa. Experimental results with MPPT control are shown in Figs. 22(a) and (b). WTG has no torque compensation, the minimum of P_e is 6.4 kW, and the minimum frequency deviation is about -0.6 Hz. The output power in Fig. 22(c) is compensated by Droop controller. The minimum of P_e is 6.4 kW, and the minimum frequency deviation is about -0.48 Hz. With the proposed MPC controller, change of P_e in Fig. 22(f) is smaller than other controllers. The minimum of P_e is 6.6 kW, and the minimum frequency deviation is about -0.44 Hz. It can be seen that the proposed torque compensation controller has a good effect on the power variation. The torque compensation abilities with MPC control are stronger than that of Droop control. The frequency change with MPC controller is the smallest.

Compared with simulation results, there are some oscillations in the experimental results, especially in the frequency restoring period, however, the overall trends are consistent. The oscillations could be caused by the weak mechanical system of the diesel generator.

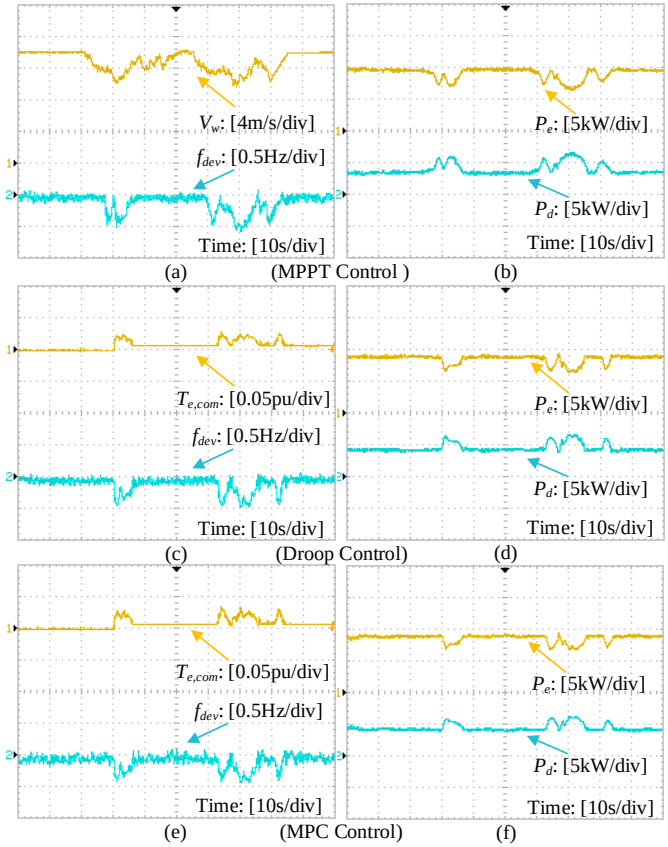

Fig. 22. Experimental results when load is constant.

VII. Conclusion

The proposed frequency regulation strategy of WTGs is implemented by coordination of generator-side converter, pitch system and torque compensation controller of a wind farm. The effectiveness of the proposed strategy is confirmed by comparison with two traditional strategies. The proposed strategy can be used for wind farm to participate in frequency regulation. The improved deloading method provides WTGs reasonable power reserves in each speed section. It is shown that frequency regulation ability in the high wind-speed section is stronger. New speed reference for the pitch system can avoid power oscillation of WTG. The MPC controller generates torque compensations for each deloaded WTG and has the ability of frequency prediction. The presented MPC controller not only enhances frequency regulation ability, but also smoothens wind farm output power and minimizes active power fluctuations. In addition, the dependence on system parameters for regulating frequency is reduced by MPC.

References

[1] M. R. Almassalkhi and I. A. Hiskens, "Model-predictive cascade mitigation in electric power systems with storage and renewables—part I: theory and implementation," *IEEE Transactions on Power Systems*, vol. 30, no. 1, pp. 67-77, 2015.

[2] M. R. Almassalkhi and I. A. Hiskens, "Model-predictive cascade mitigation in electric power systems with storage and renewables—part II: case-study," *IEEE Transactions on Power Systems*, vol. 30, no. 1, pp. 78-87, 2015.

[3] R. Sgarbossa, S. Lissandron, P. Mattavelli, R. Turri and A. Cerretti, "Analysis of ΔP -ΔQ area of uncontrolled islanding in low-voltage grids with PV generators," *IEEE Transactions on Industry Applications*, vol. 52, no. 3, pp. 2387-2396, May-June 2016.

[4] N. Nguyen and J. Mitra, "An analysis of the effects and dependency of wind power penetration on system frequency regulation," *IEEE Transactions on Sustainable Energy*, vol. 7, no. 1, pp. 354-363, 2016.

[5] Haixin Wang, Junyou Yang, Yiming Ma, Zuoxia Xing and Chen Zhe, "Model predictive control of PMSG-based wind turbines for frequency regulation in an isolated grid," *2017 IEEE 3rd International Future Energy Electronics Conference and ECCE Asia (IFEEC 2017 - ECCE Asia)*, Kaohsiung, 2017, pp. 1536-1541.

[6] A. Mitra and D. Chatterjee, "Active power control of DFIG-based wind farm for improvement of transient stability of power systems," *IEEE Transactions on Power Systems*, vol. 31, no. 1, pp. 82-93, Jan. 2016.

[7] K. V. Vidyanandan and N. Senroy, "Primary frequency regulation by deloaded wind turbines using variable droop," *IEEE Transactions on Power Systems*, vol. 28, no. 2, pp. 837-846, 2013.

[8] J. Liu, J. Wen, W. Yao and Y. Long, "Solution to short-term frequency response of wind farms by using energy storage systems," *IET Renewable Power Generation*, vol. 10, no. 5, pp. 669-678, 2016.

[9] R. M. Kamel, A. Chaouachi and K. Nagasaka, "Three control strategies to improve the microgrid transient dynamic response during isolated mode: a comparative study," *IEEE Transactions on Industrial Electronics*, vol. 60, no. 4, pp. 1314-1322, 2013.

[10] J. Dang, J. Seuss, L. Suneja and R. G. Harley, "SoC feedback control for wind and ESS hybrid power system frequency regulation," *IEEE Journal of Emerging and Selected Topics in Power Electronics*, vol. 2, no. 1, pp. 79-86, 2014.

[11] K. V. Vidyanandan and N. Senroy, "Frequency regulation in a wind–diesel powered microgrid using flywheels and fuel cells," *IET Generation, Transmission & Distribution*, vol. 10, no. 3, pp. 780-788, 2016.

[12] C. Li, E. A. A. Coelho, T. Dragicevic, J. M. Guerrero and J. C. Vasquez, "Multiagent-based distributed state of charge balancing control for distributed energy storage units in AC microgrids," *IEEE Transactions on Industry Applications*, vol. 53, no. 3, pp. 2369-2381, May-June 2017.

0093-9994 (c) 2018 IEEE. Personal use is permitted, but republication/redistribution requires IEEE permission. See http://www.ieee.org/publications_standards/publications/rights/index.html for more information.

This article has been accepted for publication in a future issue of this journal, but has not been fully edited. Content may change prior to final publication. Citation information: DOI 10.1109/TIA.2018.2817619, IEEE Transactions on Industry Applications

[13] Z. Wu, D. W. Gao, H. Zhang, S. Yan and X. Wang, "Coordinated control strategy of battery energy storage system and PMSG-WTG to enhance system frequency regulation capability," *IEEE Transactions on Sustainable Energy*, vol. 8, no. 3, pp. 1330-1343, July 2017.

[14] L. Miao, J. Wen, H. Xie, C. Yue and W. J. Lee, "Coordinated control strategy of wind turbine generator and energy storage equipment for frequency support," *IEEE Transactions on Industry Applications*, vol. 51, no. 4, pp. 2732-2742, 2015.

[15] Y. Tan, K. M. Muttaqi, P. Ciufo and L. Meegahapola, "Enhanced frequency response strategy for a PMSG-based wind energy conversion system using ultracapacitor in remote area power supply systems," *IEEE Transactions on Industry Applications*, vol. 53, no. 1, pp. 549-558, 2017.

[16] S. Zhang, Y. Mishra and M. Shahidehpour, "Fuzzy-logic based frequency controller for wind farms augmented with energy storage systems," *IEEE Transactions on Power Systems*, vol. 31, no. 2, pp. 1595-1603, 2016.

[17] J. Pahasa and I. Ngamroo, "Coordinated control of wind turbine blade pitch angle and PHEVs using MPCs for load frequency control of microgrid," *IEEE Systems Journal*, vol. 10, no. 1, pp. 97-105, 2016.

[18] Z. Wu *et al*., "Improved inertial control for permanent magnet synchronous generator wind turbine generators," *IET Renewable Power Generation*, vol. 10, no. 9, pp. 1366-1373, 2016.

[19] G. Xu and L. Xu, "Improved use of WT kinetic energy for system frequency support," *IET Renewable Power Generation*, vol. 11, no. 8, pp. 1094-1100, 2017.

[20] S. Ghosh, S. Kamalasadan, N. Senroy and J. Enslin, "Doubly fed induction generator (DFIG)-based wind farm control framework for primary frequency and inertial response application," *IEEE Transactions on Power Systems*, vol. 31, no. 3, pp. 1861-1871, 2016.

[21] S. De Rijcke, P. Tielens, B. Rawn, D. Van Hertem and J. Driesen, "Trading energy yield for frequency regulation: optimal control of kinetic energy in wind farms," *IEEE Transactions on Power Systems*, vol. 30, no. 5, pp. 2469-2478, 2015.

[22] H. Wang, Z. Chen, Q. Jiang, "Optimal control method for wind farm to support temporary primary frequency control with minimised wind energy cost" *IET Renewable Power Generation*, vol.9, no.4, pp.350-359, 2015.

[23] K. V. Vidyanandan and N. Senroy, "Primary frequency regulation by deloaded wind turbines using variable droop," *IEEE Transactions on Power Systems*, vol. 28, no. 2, pp. 837-846, 2013.

[24] M. F. M. Arani and Y. A. R. I. Mohamed, "Analysis and impacts of implementing droop control in DFIG-based wind turbines on microgrid/weak-grid stability," *IEEE Transactions on Power Systems*, vol. 30, no. 1, pp. 385-396, 2015.

[25] H. Bevrani, M. R. Feizi and S. Ataee, "Robust frequency control in an islanded microgrid: H_∞ and μ-synthesis approaches," *IEEE Transactions on Smart Grid*, vol. 7, no. 2, pp. 706-717, 2016.

[26] S. Zhang, Y. Mishra and M. Shahidehpour, "Fuzzy-logic based frequency controller for wind farms augmented with energy storage systems," *IEEE Transactions on Power Systems*, vol. 31, no. 2, pp. 1595-1603, 2016.

[27] F. Baccino, F. Conte, S. Grillo, S. Massucco and F. Silvestro, "An optimal model-based control technique to improve wind farm participation to frequency regulation," *IEEE Transactions on Sustainable Energy*, vol. 6, no. 3, pp. 993-1003, 2015.

[28] Y. Wang, J. Meng, X. Zhang and L. Xu, "Control of PMSG-based wind turbines for system inertial response and power oscillation damping," *IEEE Transactions on Sustainable Energy*, vol. 6, no. 2, pp. 565-574, 2015.

[29] B. Hoseinzadeh and Z. Chen, "Intelligent load-frequency control contribution of wind turbine in power system stability," *EUROCON, 2013 IEEE*, Zagreb, 2013, pp. 1124-1128.

[30] Z. Chen and Y. Hu, "A hybrid generation system using variable speed wind turbines and diesel units," in *Proc. IEEE Ind. Electron. Soc. Annu. Meeting Conf.*, Nov. 2003, pp. 2729-2734.

[31] Y. Hu and Z. Chen, "Modeling of frequency and power control in an autonomous power system with wind turbines and diesel generation units," *2005 IEEE/PES Transmission & Distribution Conference & Exposition: Asia and Pacific*, Dalian, 2005, pp. 1-8.

[32] H. Bevrani and S. Shokoohi, "An intelligent droop control for simultaneous voltage and frequency regulation in islanded microgrids," *IEEE Transactions on Smart Grid*, vol. 4, no. 3, pp. 1505-1513, 2013.

[33] I. U. Nutkani, P. C. Loh, P. Wang and F. Blaabjerg, "Autonomous droop scheme with reduced generation cost," *IEEE Transactions on Industrial Electronics*, vol. 61, no. 12, pp. 6803-6811, 2014.

[34] M. M. A. Abdelaziz, H. E. Farag and E. F. El-Saadany, "Optimum droop parameter settings of islanded microgrids with renewable energy resources," *IEEE Transactions on Sustainable Energy*, vol. 5, no. 2, pp. 434-445, 2014.

[35] Y. Wang, H. Bayem, M. Giralt-Devant, V. Silva, X. Guillaud and B. Francois, "Methods for assessing available wind primary power reserve," *IEEE Transactions on Sustainable Energy*, vol. 6, no. 1, pp. 272-280, 2015.

[36] A. Parisio, E. Rikos and L. Glielmo, "A model predictive control approach to microgrid operation optimization," *IEEE Transactions on Control Systems Technology*, vol. 22, no. 5, pp. 1813-1827, 2014.

[37] A. M. Ersdal, L. Imsland and K. Uhlen, "Model predictive load-frequency control," *IEEE Transactions on Power Systems*, vol. 31, no. 1, pp. 777-785, 2016.

[38] X. Liu, Y. Zhang and K. Y. Lee, "Coordinated distributed MPC for load frequency control of power system with wind farms," *IEEE Transactions on Industrial Electronics*, vol. 64, no. 6, pp. 5140-5150, 2017.

0093-9994 (c) 2018 IEEE. Personal use is permitted, but republication/redistribution requires IEEE permission. See http://www.ieee.org/publications_standards/publications/rights/index.html for more information.